ELSEVIER

Surface Science 360 (1996) 31–42

surface science

CO on Pd(110): determination of the optimal adsorption site

R. Ramprasad [a], K.M. Glassford [a,b], J.B. Adams [a,*], R.I. Masel [b]

[a] *Department of Materials Science and Engineering, University of Illinois, Urbana, IL 61801, USA*
[b] *Department of Chemical Engineering, University of Illinois, Urbana, IL 61801, USA*

Received 10 January 1996; accepted for publication 8 February 1996

Abstract

We present ab initio pseudo-potential plane-wave total-energy calculations for the geometric and electronic structure of the CO-covered Pd(110) surface. Our calculations were performed within the local-density approximation (LDA) of density functional theory (DFT). There has been some controversy as to whether CO prefers to adsorb at a bridge or on-top site when exposed to Pd(110). Total energy calculations for a CO monolayer adsorbed at the on-top and bridge adsorption sites revealed the bridge site adsorption to be favored by 0.59 eV per CO molecule. The preferential adsorption of CO to the bridge site was further corroborated by our band-structure calculations, with only the bridge site results being in good agreement with recent inverse photoemission experiments.

Keywords: Carbon monoxide; Catalysis; Chemisorption; Density functional calculations; Palladium

1. Introduction

The majority of industrial chemical and biochemical processes rely quite heavily on catalytic materials. In automotive industries, catalytic treatment of the automobile exhaust gases has been a standard feature in the USA since 1975 in order to control the amount of carbon monoxide, hydrocarbons and nitric oxide in the exhaust gases of vehicles. At stoichiometric air/fuel ratios, this is accomplished by three-way catalysts (TWCs) which contain the expensive noble metals Pt, Pd and Rh. Pt and Pd are primarily used for CO and hydrocarbon oxidation while Rh is found to be most effective for NO_x reduction. Three-way catalysts, while being very efficient at treating exhaust emissions from engines operating under a stoichiometric air/fuel ratio, perform very poorly when used in conjunction with lean-burn engines. A good understanding of the TWC is necessary both to improve present-day catalysts and to develop efficient lean-burn catalysts. The scientific literature is replete with articles concerning work in the last twenty years on TWCs [1], as well as related chemisorption studies of the relevant gases on ideal single crystal surfaces [2–11]. In the present study, we perform a theoretical investigation of CO chemisorption at saturation coverage on the Pd(110) surface. This is the first step in understanding how and why TWCs function.

There have been a variety of experimental studies on CO chemisorption on transition metal surfaces, in particular the (111), (110), (210) and the (100) surfaces of Pt, Pd and Ni [2–11]. In all but the (110) surfaces, saturation coverages were less than

* Corresponding author. Fax: +1 217 2446917; e-mail: jba@uiuc.edu.

PII S0039-6028(96)00600-0

a monolayer of CO; also, there is general agreement as to what the geometric structure of the chemisorbed phase is in all cases except the (110) surface. The CO-covered (110) surface of Pd has been studied by inverse photoemission [6] and also by low-energy electron diffraction (LEED) [7]. CO forms a densely packed ordered monolayer on these surfaces with the CO molecules adsorbed along the densely packed surface atom chains in the $[1\bar{1}0]$ direction. This results in an alternating tilt of the CO molecules in the [001] direction perpendicular to the atom rows, due to the CO–CO repulsion giving rise to a (2×1)p2mg superstructure with two molecules per unit cell.

Ambiguities still exist regarding the details of the geometry of this structure, especially the site of the CO molecule (bridge or on-top surface site). For the case of (2×1)CO/Pd(110), Ertl et al. [8] placed the CO in high-coordination B_5 sites, but Chesters et al. [9] showed by electron energy-loss spectroscopy (EELS) that CO adsorbs preferentially at B_2 bridge sites. More recently, a reflection–absorption infrared spectroscopy (RAIRS) study [10] concluded, by comparison of the surface vibrational CO stretching frequency with organometallic data, that CO is two-fold bridge-coordinated. A photoelectron diffraction (PD) study [11] also came to this conclusion, whereas a recent LEED study [7] indicated an on-top coordination site for CO. In addition to the site preference of CO, experimental studies disagree on the magnitude of the lateral shift of the C atom, the angle of tilt of the C–O bond with respect to the surface normal, and whether the metal–C–O bond is linear or kinked. There have not been many relevant theoretical calculations of CO chemisorption on Pd surfaces, or even on Ni or Pt surfaces which are expected to behave similarly to the Pd surfaces. Wimmer et al. [12] performed full-potential linearized augmented plane-wave (FLAPW) calculations of CO on Ni(001) coadsorbed with K or S, and Wong and Hoffmann [13] studied CO chemisorption on Ni(111), Pd(111) and Pt(111) using the extended Huckel method. We [14] had earlier carried out calculations based on density functional theory (DFT) to determine the geometric parameters for (2×1)CO/Pd(110) assuming an on-top CO adsorption site. More recently, Hu et al. [15] performed DFT calculations (within both the local density and generalized gradient approximations) for CO on Pd(110) and observed that the bridge site is preferred over the on-top site for CO chemisorption [15]. They also demonstrated, using orbital mixing considerations [15], that the traditional Blyholder model [16] oversimplifies the interaction between the CO molecule and transition-metal atoms.

In the present study, we provide more conclusive evidence regarding CO site preference, confirming the work of Hu et al. [15]; our calculations were based on DFT within the local-density approximation (LDA). The organization of the paper is as follows: we describe the methods used in our calculations in Section 2. In Sections 3 and 4, we present our results for bulk Pd, the clean Pd (110) surface and examine the geometric and electronic structure of the CO covered Pd (110). Section 5 summarizes our results.

2. Methods of calculation

The theoretical basis of our calculations is density functional theory (DFT) [17,18] which, in principle, is an exact theory. It shifts the emphasis from the wave-function to the electron density, and states that the total energy of a system is a unique functional of the electron density [18a]. Present-day implementations are based on some form of approximation to this theory, for instance, the local-density approximation (LDA) [18,19] to treat the exchange-correlation contributions to the energy. It is this type of implementation that we have used in the present work. The Ceperley–Alder exchange-correlation potential [20] as parameterized by Perdew and Zunger [21] was used, and the Kohn–Sham [18] equations were iterated to self-consistency using a plane-wave basis set.

Soft ab initio relativistic pseudo-potentials were generated for Pd, C and O in order to avoid explicit treatment of the core electrons using the method of Troullier and Martins [22] and were transformed, for computational ease, using the separation technique of Kleinman and Bylander [23]. The lowest-order relativistic corrections to the atomic energies are $O(\alpha^4Z^4)$, where α is the

fine structure constant and Z is the atomic number. So, for Pd, which is a 4d transition metal atom with atomic number 46, we anticipate noticeable relativistic effects to manifest, at least for the core electrons. Hence, our atomic pseudo-potentials were generated by inverting the relativistic Kohn–Sham equations so that the relativistic effects felt in the core region are adequately incorporated in the pseudo-potentials. We discuss this point again in Section 3. The Pd pseudopotential was generated from the atomic ground-state configuration ($4d^{10}5s^{0}5p^{0}$) with radial cut-offs of 2.25, 2.60 and 2.00 au for the s, p and d components. The 5s component was chosen as the local component. The C pseudopotential [22] was generated from its atomic ground-state configuration ($2s^{2}2p^{2}$) with radial cut-offs of 1.50 and 1.54 au for the s and p components. Here, the 2p component was chosen as the local component. The O pseudo-potential was obtained from Ref. [24]. The d component was neglected in the cases of C and O as the 3d atomic energies for both these atoms were too high in energy compared to that of the 2s and the 2p states. Our choices of the local potentials did not introduce any ghost states [25]. In order to ensure good transferability of the pseudo-potentials over a wide energy range, we calculated logarithmic derivatives of the radial component of the pseudo wave-function over a wide energy range and compare them with our all-electron calculations, as shown in Fig. 1, where arrows indicate atomic eigenvalues calculated from all-electron calculations for the reference configurations mentioned above. By construction, the pseudo-potential eigenvalues are equal to the all-electron results. As can clearly be seen, our pseudo-potential calculations show excellent agreement with our all-electron calculations for both Pd and C below 1 Ry. One-electron energies less than 1 Ry are the ones that are physically significant and important in the present study. It can also be seen in Fig. 1 that spurious ghost states are absent.

We did not include self-interaction corrections [26–28] to our approximate (LDA) exchange-correlation functional as it has been generally accepted [27] that these corrections are not important for metallic systems whose wave-functions are delocalized Bloch functions. We also found that

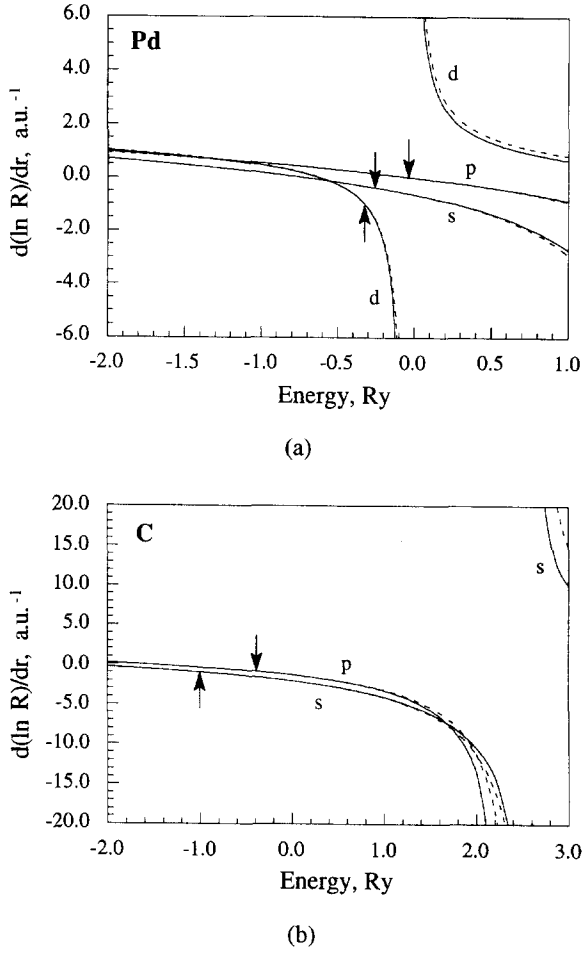

Fig. 1. Logarithmic derivatives of the radial components of the pseudo wave-functions (dashed lines) and the all electron wave functions (solid lines) for different angular momentum components for (a) atomic Pd at a radius of 2.58 au, and (b) atomic C at a radius of 1.46 au.

core corrections [29,30] did not significantly change our results.

Analysis of the convergence of the calculated total energy per primitive unit-cell of bulk Pd and diamond with respect to the plane-wave cut-off energy showed that plane-waves up to an energy of 50 Ry yielded well-converged total energies. Increasing the plane-wave cut-off energy to 90 Ry decreased the total-energy per primitive cell by only 0.001 Ry in the case of bulk Pd and by 0.004 Ry in the case of diamond. However, for O, convergence was achieved only at a plane-wave

cut-off energy of 64 Ry. As a result, we used a plane-wave cut-off energy of 50 Ry when studying bulk Pd and the clean Pd(110) slab, and used 64 Ry when studying the CO-covered Pd(110) surface. We used the supercell method in all our calculations. Clean Pd(110) was modelled with three layers. CO-covered Pd(110) was modelled by assuming that both sides of the three-layer slab were covered with CO. This resulted in a supercell belonging to a space group with more symmetry operations than the supercell that would have resulted if we had covered only one side of the slab with CO. This was desirable as our code was equipped to make use of symmetrized plane-waves to speed up calculations. At self-consistency, the Fourier components of the potential differed by less than 0.1 mRy from the previous iteration, and the total-energy was stable to within 10^{-6} Ry per atom or better between iteration cycles. Self-consistency was typically reached in five iterations in the case of bulk Pd, in 24 iterations in the case of the clean Pd(110) surface, and in about 40 iterations in the case of CO-covered Pd(110). Geometry optimizations were performed using a conjugate gradient minimization. All atoms were allowed to relax in an unconstrained manner till each component of the forces was less than 0.007 Ry au^{-1}. The supercell sizes were 7.36 au × 5.20 au × 15.61 au for the clean Pd(110) calculations (over 10 au vaccuum) and 7.36 au × 10.40 au × 20.82 au for the CO-covered Pd(110) calculations (over 8 au vacuum). We used six special $\boldsymbol{k}$ points (per irreducible wedge of the Brillouin zone) in studying bulk Pd, four $\boldsymbol{k}$ points in studying the clean Pd(110) surface, and two $\boldsymbol{k}$ points in studying the CO-covered Pd(110) surface. For bulk Pd, increasing the number of special $\boldsymbol{k}$ points to 19 decreased the total energy by only 0.003 Ry per atom. For the clean and CO-covered Pd(110) surface, the number of $\boldsymbol{k}$ points we used were found to yield well-converged results.

3. Results

3.1. Bulk Pd

Bulk Pd occurs in an fcc crystal structure. We have performed calculations to determine the structural, cohesive, elastic and electronic properties of bulk Pd. This served as a test of our Pd pseudopotential. The ground state of the system is obtained by minimizing the total energy per atom of the fcc structure with respect to the lattice parameter. The ground-state structural and elastic properties are determined by fitting the theoretical values of energy and volume to an integrated equation of state. Here, we have used the Birch–Murnaghan form [31]. In Table 1, we compare the calculated structural, cohesive and elastic properties with the corresponding experimental values

Table 1
Structural, cohesive and elastic properties of bulk Pd

Property	This work[a]	SR[b] [35]	NR[c] [35]	CC[d]	Experiment
a_0[e] (Å)	3.89	3.88	3.94	3.91	3.89 [32]
E_{coh}[f] (eV)	4.62	4.56	3.61	4.54	3.91 [33]
B_0[g] (GPa)	210.5	215	180	207.3	195.5 [34]
B_0'[h]	5.95	–	–	5.89	–

[a] Results of the present work without core corrections.
[b] SR = scalar relativistic.
[c] NR = non-relativistic.
[d] Results of the present work with core corrections included.
[e] a_0 is the lattice constant.
[f] E_{coh} is the cohesive energy.
[g] B_0 is the bulk modulus.
[h] B_0' is the first pressure derivative of the bulk modulus.

[32–34] and also with other non-relativistic and scalar-relativistic calculations [35]. It can be seen that the calculated lattice constant is in excellent agreement with experiment. The bulk modulus is about 8% higher, which is reasonable. The cohesive energy is about 18% higher than the corresponding experimental values, which is typical of LDA. We also give the value for the first pressure derivative of the bulk modulus B_0'. It is interesting to note that our results are in closer agreement to other scalar-relativistic (SR) calculations than with non-relativistic (NR) calculations. This is because we constructed our pseudo-potentials from relativistic atomic calculations. Although our solid calculations were non-relativistic, the relativistic effects that manifest in the core region are built into the pseudopotentials. In Fig. 2, we show the calculated band-structure of bulk Pd. We compare it with an all-electron, scalar-relativistic augmented plane-wave (APW) band-structure calculation performed earlier [36] (shown as dots in Fig. 2) and find that the agreement is excellent.

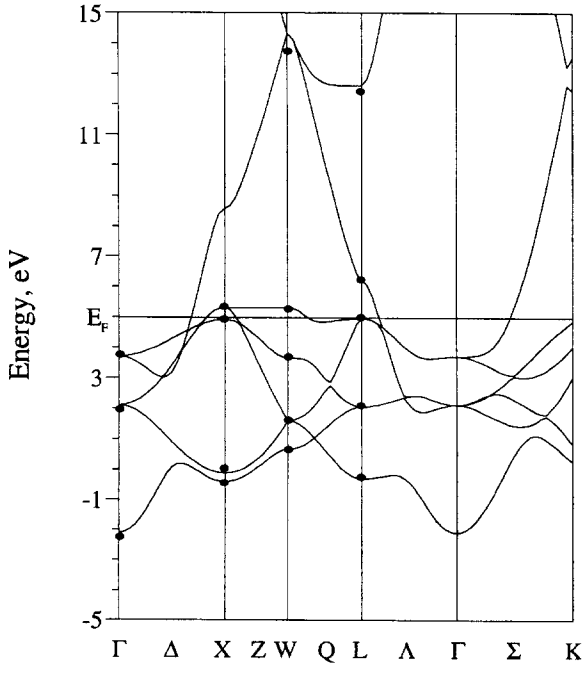

Fig. 2. Calculated bulk band structure of Pd. Dots indicate results from a previous all-electron, scalar-relativistic augmented plane-wave (APW) calculation [36]. The Fermi level (E_F) is indicated by a line.

In the case of transition-metal atoms, there is also the question of whether or not a core correction [29,30] to the exchange-correlation potential is necessary. It is generally believed that a core correction is necessary whenever there is significant overlap between the valence and core charge densities. As is evident from Fig. 3, there is significant overlap between the valence and core charge densities. The core charge density shown in Fig. 3 is from a Gaussian core model, which approximates the core charge over the region in which the core and valence charge densities overlap. We then performed bulk Pd calculations, this time with the core corrections included and we show the results in Table 1. We found that the core corrections show no significant improvement over our original results. This was not surprising, as core corrections produce significant changes only for the 3d transition metals as in these metal atoms, there is no inner d shell to repel the valence d orbital. However, since Pd is a 4d transition metal with a core consisting of a 3d orbital, these core corrections should not be important (as we found). Hence, all subsequent calculations were done without core corrections.

3.2. Clean Pd(110)

Clean Pd(110) forms an unreconstructed channeled surface. We chose a three-layer Pd(110) slab

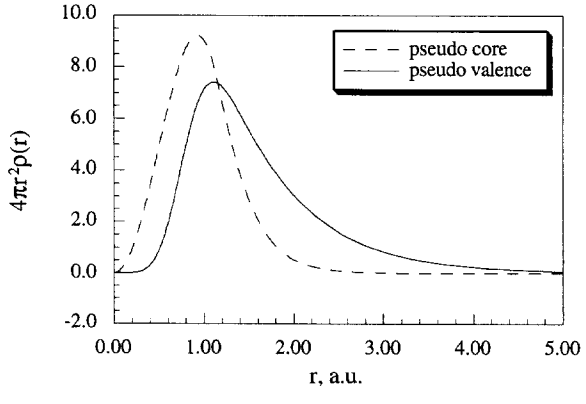

Fig. 3. Gaussian core (dashed line) and valence (solid line) radial charge densities [$4\pi r^2\rho(r)$]; in the Gaussian core model, the core charge density is approximated in the region in which the core and the valence charge densities overlap.

as a model for the Pd(110) surface. Experiments [37] indicate that for the Pd(110) surface, the interlayer relaxation does not go beyond the second interlayer spacing. So, although we expect the first interlayer relaxation for clean Pd(110) to differ quantitatively from experiments, we do not anticipate the geometric details of our CO/Pd(110) calculations to change significantly if we use a thicker slab. Also, Hu et al. [15] have shown that their CO/Pd(110) results did not change quantitatively when they replaced their frozen three-layer Pd(110) slab with a four-layer Pd(110) slab. As we use periodic boundary conditions along all three dimensions of the unit cell, the optimum unit-cell height in the direction perpendicular to the (110) surface is to be determined, for which the total-energy of the slab is well converged. We found that a unit-cell height of 15.61 au (six times the bulk (110) interplanar spacing) gives good total-energy convergence. Increasing the unit cell height to 20.82 au (eight times the bulk interplanar spacing) decreased the total energy by only 0.002 Ry per atom. We next determined the surface relaxation between the first and the second layers, which was done by minimizing the total energy of the slab with respect to variations in the first interlayer spacing. We found that the total energy was a minimum for an interlayer spacing of 2.54 au, implying a -2.3% relaxation (contraction) of the first interlayer spacing. The surface energy for this relaxed structure was 1.60 J m^{-2}. Considering that the slab we have studied is only three layers thick, these calculated values are in reasonably good agreement with the experimental first interlayer relaxation value [37] of $-6.0 \pm 2.0\%$, and in excellent agreement with the experimental 0 Kelvin (extrapolated) surface energy of 1.63 J m^{-2} [38].

3.3. CO/Pd(110)

The CO-covered Pd(110) surface at saturation coverage is an ordered structure with a (2×1)p2mg superstructure with two molecules per surface unit cell. Fig. 4a shows the side view (along the $[1\bar{1}0]$ direction) and Figs. 4b and 4c show the top view for on-top and bridge CO adsorption, respectively. For reasons of symmetry, as mentioned earlier, we placed CO on both sides of the three-layer Pd(110) slab.

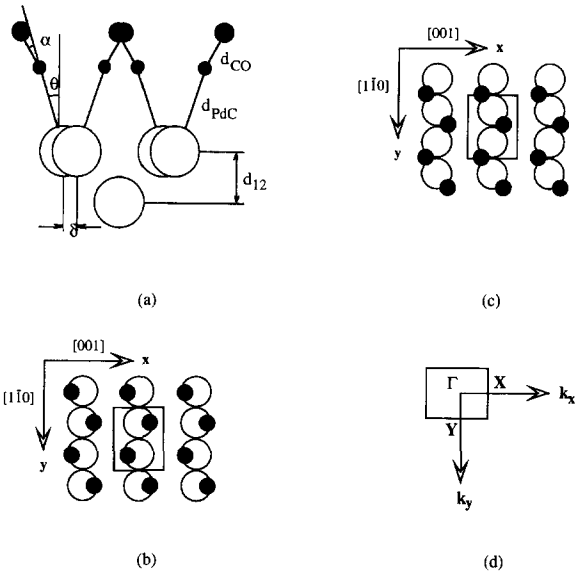

Fig. 4. (a) Side view (along the $[1\bar{1}0]$ direction) of CO/Pd(110) geometry showing the relevant structural parameters. (b) Top view of the CO/Pd(110) (2×1)p2mg superstructure (on-top CO adsorption) showing the surface unit cell; open circles indicate Pd atoms and solid circles schematically represent CO molecules. (c) As (b), but for bridge-site CO adsorption. (d) The first Brillouin zone of the surface structure of (b) and (c), showing the high-symmetry points.

3.3.1. Geometric details

We have minimized the total-energy with respect to six structural parameters (for both possible CO adsorption sites), i.e. the C–O bond length d_{C-O}, the Pd–C bond length d_{Pd-C}, the Pd(110) interlayer spacing d_{12}, the angles θ and α (as defined in Fig. 4a) and the lateral reconstruction shift of the first layer Pd atoms δ. All these parameters are shown in Fig. 4a. In Table 2, we compare our calculated parameters for on-top CO chemisorption, the LEED experimental values [7] (which predict an on-top equilibrium adsorption site for CO) and the theoretical calculations of Hu et al. [15]. From Table 2, it is evident that d_{C-O}, d_{12}, α and δ are all well within the experimental error. The calculated θ value is larger than the experimental value. The calculated d_{Pd-C} value is significantly shorter than the corresponding experimental value,

Table 2
Parameters (as defined in Fig. 4a) of the CO-covered Pd(110) slab for on-top site adsorption

Parameter	This work	Hu et al. [15] (LDA)	Hu et al. [15] (GGA)	TLEED experiment [7]
d_{C-O} (Å)	1.15	1.14	1.14	1.16 ± 0.04
d_{Pd-C} (Å)	1.91	1.94	1.96	2.11 ± 0.06
d_{12} (Å)	1.33	–	–	1.32 ± 0.05
θ (°)	19.7	12.3	12.4	11 ± 4
α (°)	1.4	−1.6	−0.3	2 ± 5
δ	0.006	–	–	0.04 ± 0.11

due to the thinness of the slab (which results in a poorer supply of electronic charge). The differences between the calculated and experimental values are also in part due to interactions between the periodic images of the polarized CO molecules, and also between CO molecules on either sides of the slab of the same unit cell. All the bond lengths are in good agreement with the results of Hu et al., but the bond angles differ considerably, presumably due to the neglect of substrate relaxations by Hu et al. We also mention, in passing, that as per the results of Hu et al., the structural parameters do not change significantly when generalized gradient approximation (GGA) corrections are added to the LDA, although this is not the case with relative or total energies.

We also performed a geometry optimization for the other possible adsorption site for CO, i.e. the short bridge site (Fig. 4c). The geometric details are shown in Table 3 along with the photoelectron diffraction (PD) experimental results [11] (which predict a bridge adsorption site for CO) and the LDA and GGA results of Hu et al. [15]. As in the case of on-top adsorption, our values for d_{Pd-C} and θ differ from the corresponding experimental results, and as before, our bond lengths are in good agreement with the results of Hu et al., but our bond angles differ considerably from their results.

3.3.2. Relative energies

We found that the bridge site was energetically favored over the on-top site by 0.59 eV per CO molecule. This is in agreement with the calculations of Hu et al. [15] mentioned above, which also predict that the bridge site is energetically favored by 0.47 eV within the local density approximation (LDA), and by 0.33 eV within the generalized gradient approximation (GGA).

3.3.3. Surface band structure

We now shift our attention to the electronic structure of the CO/Pd(110)-p2mg superstructure. Figs. 4b and 4c show the ordered (p2mg symmetry) surface structure for CO adsorbed to the on-top and bridge adsorption sites, respectively, along with the surface unit-cell. The corresponding first Brillouin zone is shown in Fig. 4d. We use the fragment molecular orbital (FMO) analysis of Hoffmann [39,40] as applied to periodic systems to study the electronic structure of CO/Pd(110). The band structure of the ordered, double-layered

Table 3
Parameters (as defined in Fig. 4a) of the CO-covered Pd(110) slab for bridge-site adsorption

Parameter	This work	Hu et al. [15] (LDA)	Hu et al. [15] (GGA)	PD experiment [11]
d_{C-O} (Å)	1.16	1.15	1.15	–
d_{Pd-C} (Å)	2.01	2.05	2.08	1.8 ± 0.1
d_{12} (Å)	1.37	–	–	–
θ (°)	24.9	11.9	15.7	5 ± 5
α (°)	−1.3	0.5	−2.2	–
δ	0	–	–	–

CO array without the Pd–CO interaction is shown in Fig. 5a, and that with the Pd–CO interaction turned on is shown in Fig. 5b (on-top adsorption) and Fig. 5c (bridge adsorption). We restrict ourselves to only the bands formed from the frontier molecular orbitals and have not shown the projected bulk band-structure. Since LDA methods are known to poorly describe bandgaps (and band energies of unoccupied bands with respect to the Fermi energy), we uniformly shifted the calculated bands to best fit the experimental data. The band structure for the on-top site adsorption was shifted up by about 0.8 eV (Fig. 5d) and that for bridge-site adsorption was shifted up by about 0.5 eV

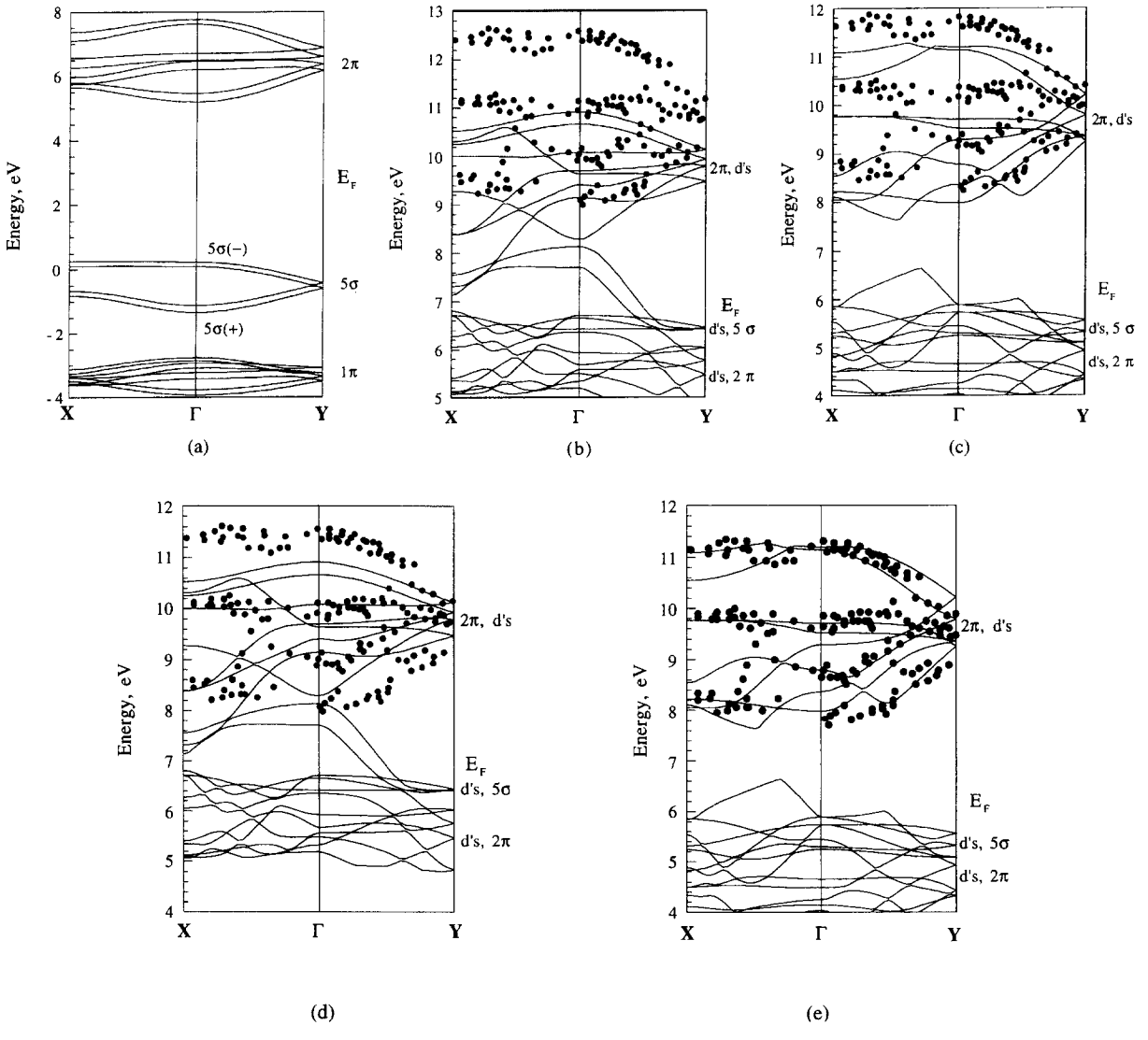

Fig. 5. Surface band-structure of the (2×1)p2mg ordered CO array. (a) Without the CO–Pd interaction; $5\sigma(+)$ and $5\sigma(-)$ bands are derived from bonding and anti-bonding combinations within the surface unit cell of the CO 5σ molecular orbital. (b) With the CO–Pd interaction turned on for CO adsorbed to the on-top site. (c) With the CO–Pd interaction turned on for CO adsorbed to the bridge site; bands arising from the bonding and antibonding combinations of the CO 2π-derived and Pd d-bands, and bands arising from the antibonding combination of CO 5σ-derived and Pd d-bands are shown. The Fermi energy level is indicated "E_F". (d) As (b) but with the calculated bands shifted up by 0.8 eV. (e) As (c) but with the calculated bands shifted up by 0.5 eV.

(Fig. 5e). We clearly see a better agreement between the calculated band-structure for the bridge-site adsorption case than for the on-top adsorption case. This leads us to believe that the experimentally observed bands are due to CO adsorbed to the bridge site. Thus, we have arrived at the conclusion that CO prefers to bind to the bridge sites on Pd(110) by two very different analyses, i.e. total-energy and unoccupied band-structure considerations.

4. Further discussion of band structure

In what follows, we first attempt to describe some of the important features of Fig. 5a, before moving on to Figs. 5b (or 5d) and 5c (or 5e). Each CO molecule gives rise to two 1π (occupied) orbitals, one 5σ (occupied) orbital and two 2π (unoccupied) orbitals. The surface unit-cell (Fig. 4b) has two CO molecules and so, we should see four 1π, two 5σ and four 2π bands, half of which are bonding combinations, and the other half anti-bonding combinations of the appropriate molecular orbitals of the two CO molecules within the unit cell. We, on the other hand, see twice as many bands in Fig. 5a as we have covered both sides of our Pd slab with CO, and the interaction between CO molecules (which are, for the most part, long-range dipole–dipole interactions) on different surfaces further splits up each of the expected bands into two closely spaced bands, as can be seen in Fig. 5a. Had we used a thick enough slab, we would have seen the right number of bands, but in this case each of the bands would have been doubly degenerate at all points in the Brillouin zone. From this point, unless otherwise stated, we ignore the splitting of the bands due to interaction between CO molecules in different layers.

It is evident from Fig. 5a that there is no degeneracy between π_x- and π_y-derived bands. It is interesting to note that the bands arising from the bonding and anti-bonding combinations of a certain molecular orbital are degenerate at the Y point but not at the X point. If we follow the bands in $\boldsymbol{k}$ space (Fig. 5a) along Γ–Y, we see, for instance, that the $5\sigma(+)$ band increases in energy, while the $5\sigma(-)$ band decreases in energy until it

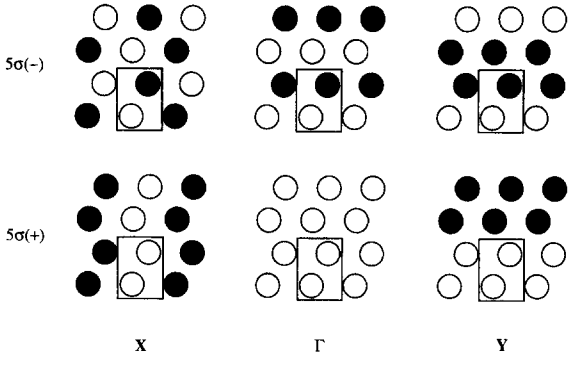

Fig. 6. Schematic real-space representation of the CO 5σ-derived wave-functions at three high-symmetry points of the (2×1)p2mg surface Brillouin zone. The surface unit-cell is shown.

becomes degenerate at Y. The reason for this is pretty clear if we examine the nature and symmetry properties of the wave-functions at these special points in the Brillouin zone. In Fig. 6, we show schematically two-dimensional, periodic wave-functions of σ symmetry at the high-symmetry points of the (2×1)p2mg structure (the same arguments can be used to explain the degeneracies that manifest in bands with π symmetry). In the bottom panels, we show wave-functions which are bonding (+) within the unit cell; the top panels show wave-functions which are anti-bonding (−) within the unit cell. From Fig. 6, we see that, for the $5\sigma(+)$ at the Y point, we have a wave-function with phase changes only between double rows in the $[1\bar{1}0]$ direction. For the $5\sigma(-)$ case, the same wave-function results at the Y point, causing the bands to be degenerate at that point. For the X point, however, there is no such symmetry restriction; the spatial separation between sites of equal phase is more for the anti-bonding case than it is for the bonding case, and so the wave-functions are not degenerate at this point.

Before we move on to a discussion of Figs. 5b and 5c, we briefly review the current status of understanding regarding bonding in a transition-metal carbonyl [14]. In the case of a PdCO cluster, the CO 5σ and 2π orbitals combine in a bonding and antibonding fashion with the metal d-orbitals. The 5σ–d interaction is a four-electron two-orbital interaction which results in two fully occupied

orbitals (5σ–d bonding, primarily 5σ, and 5σ–d anti-bonding, primarily d), and so is a net destabilizing interaction. The 2π–d interaction is a four-electron four-orbital interaction which results in two fully occupied orbitals (2π–d bonding, primarily d) and two unoccupied orbitals (2π–d anti-bonding, primarily 2π) and so stabilizes the cluster (though the CO molecule is itself partially destabilized, as the initially unoccupied 2π orbitals have picked up some electron density). Ideas very similar to these were originally proposed by Blyholder [16].

When we move from the cluster to the surface case, we notice similarities, but there are differences as well. The frontier orbitals of CO, i.e. those corresponding to the 5σ and 2π bands, interact with those of the Pd d-bands of suitable symmetry. Using the theory of group representations, one can classify levels of like symmetry at various points in the Brillouin zone according to the representation they transform. Since in our case the interaction between CO molecules in different layers complicates the band structure, we do not give detailed symmetry assignments to the bands. Rather, we give tentative assignments to groups of bands reminiscent of their origin and analogous to the cluster case (such assignments are meaningful only at certain special points in the Brillouin zone, like the Y point, in the present case). We show only the bands resulting from the antibonding combination of the 5σ–d interaction and the bonding and anti-bonding combination of the 2π–d interaction. The reason we say that these assignments are only tentative is due to the fact that no band is entirely 5σ–d or 2π–d; for one thing, there is the possibility of little admixtures of sp(Pd) character in these bands, but more importantly, there could be hybridization between some 5σ and 2π bands, depending on whether they belong to the same representation and if they are in proximity with each other, either energetically or spatially. Just as in the PdCO cluster case, we see in Figs. 5b and 5c, that the band corresponding to the bonding combination of 2π–d interaction is fully occupied (barring hybridization), and that corresponding to the anti-bonding combination of the 2π–d interaction is fully unoccupied. The antibonding combination band of the 5σ–d interaction is, however, only partially occupied as the Fermi surface goes clean through the band (we note once again that the "5σ–d" band is predominantly 5σ–d in character, with varying small admixtures of sp(Pd), 2π and 4σ at different points in the Brillouin zone). Here, we see an essential difference between bonding of a molecule to a cluster and to a surface. Our results also indicate that the Blyholder model [16] is over-simplistic, as emphasized by others elsewhere [15, 41–43].

5. Summary and conclusions

We have reported self-consistent calculations performed within the LDA framework of DFT using soft ab initio pseudo-potentials and a plane-wave basis. Our results can be summarized as follows.

5.1. Bulk Pd

Our bulk Pd calculations yielded results that are in reasonable agreement with experiments. Our calculated lattice constant for Pd was less than 1% different from the experimental value, the bulk modulus was about 8% higher and the cohesive energy was about 18% higher than the corresponding experimental values. The calculated band-structure for bulk Pd were in excellent agreement with previous scalar relativistic calculations.

5.2. CO/Pd(110) surface geometry

We have compared our geometric parameters to experiments and earlier calculations and found that the level of agreement varied. For instance, the Pd–C bond length was too small (on-top case) or too large (bridge case) when compared to the relevant experiments (presumably in part due to the thinness of our slab), but was in good agreement with the calculation of Hu et al. [15]. Also, the calculated CO bending angle was different from both the earlier theoretical and experimental estimates. Other geometric parameters were in good agreement with previous experimental and theoretical values.

5.3. Site preference

We also performed total-energy and surface band-structure calculations to determine the equilibrium adsorption site for CO on Pd(110): (i) total energy considerations indicated that the bridge site was preferred for CO chemisorption by 0.59 eV relative to the on-top CO adsorption case, and (ii) surface band-structure calculations for both on-top and bridge adsorption cases were performed and the unoccupied bands were compared to inverse photoemission results. It was quite apparent that the calculated band-structure for the bridge-site adsorption case was in better agreement with the experimental band-structure. Based on two different considerations, i.e. total-energy and band-structure considerations, we find that CO, at saturation coverage, preferentially adsorbs on the bridge site of the Pd(110) surface.

Acknowledgements

This work was supported by NSF under Grant No. NSF-1-5-30897. We would like to thank the National Center for Supercomputing Applications (NCSA), the Pittsburgh Supercomputing Center (PSC), the University of Illinois Materials Research Laboratory Center for Computation (MRLCFC). We also would like to thank Dr. Norman Troullier (IBM) for sharing his plane-wave code with us, and Dr. Kenneth Hass (Ford Motor Company) for stimulating discussions.

References

[1] J.T. Kummer, J. Phys. Chem. 90 (1986) 4747, and references therein.
[2] J.C. Campuzano, in: The Chemical Physics of Solids and Surfaces, Vol. 4, Eds. D.A. King and D.P. Woodruff, ch. 4, and references therein.
[3] G.A. Somarjai, in: Introduction to Surface Chemistry and Catalysis (Wiley, New York, 1994).
[4] H. Kuhlenbeck, M. Neumann and H.-J. Freund, Surf. Sci. 173 (1986) 194.
[5] H. Kuhlenbeck, H.B. Saalfeld, U. Buskotte, M. Neumann, H.-J. Freund and E.W. Plummer, Phys. Rev B 39 (1989) 3475.
[6] E. Bertel, N. Memmel, G. Rangelov and U. Bischler, Chem. Phys. 177 (1993) 337.
[7] A. Wander, P. Hu and D.A. King, Chem. Phys. Lett. 201 (1993) 393.
[8] G. Ertl, H. Conrad, J. Koch and E.E. Latta, Surf. Sci. 43 (1974) 462.
[9] M.A. Chesters, G.S. McDougall, M.E. Pemble and N. Sheppard, Surf. Sci. 164 (1985) 425.
[10] R. Raval, M.A. Harrison and D.A. King, Surf. Sci. 211/212 (1989) 61.
[11] A. Locatelli, B. Brena, S. Lizzit, G. Comelli, G. Cautero, G. Paolucci and R. Rosei, Phys. Rev. Lett. 73 (1994) 90.
[12] E. Wimmer, C.L. Fu and A.J. Freeman, Phys. Rev. Lett. 55 (1985) 2618.
[13] Y.T. Wong and R. Hoffmann, J. Phys. Chem. 95 (1991) 859.
[14] R. Ramprasad, K.M. Glassford and J.B. Adams, MRS Vol. 344 in: Materials and Processes for Environmental Protection.
[15] P. Hu, D.A. King, S. Crampin, M.-H. Lee and M.C. Payne, Chem. Phys. Lett. 230 (1994) 501;
P. Hu, D.A. King, M.-H. Lee and M.C. Payne, Chem. Phys. Lett. 246 (1995) 73.
[16] G. Blyholder, J. Phys. Chem. 68 (1964) 2772.
[17] R.G. Parr and W. Yang, in: Density Functional Theory of Atoms and Molecules (Oxford, New York, 1989).
[18] P. Hohenberg and W. Kohn, Phys. Rev. 136 (1964) B864. W. Kohn and L.J. Sham, Phys. Rev. 140 (1965) A1133.
[19] O. Gunnarsson and I. Lundquist, Phys. Rev. B 13 (1976) 4274.
[20] D.M. Ceperley and B.J. Alder, Phys. Rev. Lett. 45 (1980) 566.
[21] J.P. Perdew and A. Zunger, Phys. Rev. B 23 (1981) 5048.
[22] N. Troullier and J.L. Martins, Solid State Commun. 74 (1990) 613; Phys. Rev. B 43 (1991) 1993.
[23] L. Kleinman and D.M. Bylander, Phys. Rev. Lett. 48 (1982) 1425.
[24] K.M. Glassford and J.R. Chelikowsky, Phys. Rev. B 46 (1992) 1284.
[25] X. Gonze, P. Kackell and M. Scheffler, Phys. Rev. B 41 (1990) 12264.
[26] J.P. Perdew, Chem. Phys. Lett. 64 (1979) 127.
[27] Z. Szotek, W.M. Temmerman and H. Winter, Phys. Rev. B 47 (1993) 4029.
[28] B.G. Johnson, C.A. Gonzales, P.M.W. Gill and J.A. Pople, Chem. Phys. Lett. 221 (1994) 100.
[29] S.G. Louie, S. Froyen and M.L. Cohen, Phys. Rev. B 27 (1982) 3111.
[30] H.S. Greenside and M. Schluter, Phys. Rev. B 28 (1983) 535.
[31] F. Birch, J. Geophys. Res. 57 (1952) 227.
[32] R.W.G. Wycoff, in: Crystal Structures, 2nd Ed. Vol. 1, p. 10.
[33] C. Kittel, in: Introduction to Solid State Physics (Wiley, New York) p. 55.
[34] G. Simmons and H. Wang, in: Single Crystal Elastic Constants, p. 233.

[35] C. Elsasser, N. Takeuchi, K.M. Ho, C.T. Chan, P. Braun and M. Fahnle, J. Phys.: Condens. Matter 2 (1990) 4371.
[36] D.A. Papaconstantopoulos, in: Handbook of the Band Structure of Elemental Solids (Plenum, New York, 1986).
[37] C.J. Barnes, M.Q. Ding, M. Lindroos, R.D. Diehl and D.A. King, Surf. Sci. 162 (1985) 59.
[38] W.R. Tyson, Can. Metall. Q. 14 (1975).
[39] R. Hoffmann, in: Solids and Surfaces: A Chemist's View of Bonding in Extended Structures (New York, 1988).
[40] R. Hoffmann, Rev. Mod. Phys. 60 (1988) 601.
[41] S. Ishi, Y. Ohno and B. Viswanathan, Surf. Sci. 161 (1985) 349.
[42] B. Gumhalter, K. Wandelt and Ph. Avouris, Phys. Rev. B 37 (1988) 8048.
[43] P.S. Bagus, C.J. Nelin and C.W. Bauschlicher, Jr., Phys. Rev. B 28 (1983) 5423.